DEVELOPING A MODE II FRACTURE MODEL FOR COMPOSITE LAMINATES

C.E. Rogers, E.S. Greenhalgh and P. Robinson

The Composites Centre, Dept. of Aeronautics, Imperial College London, UK
charlotte.rogers03@imperial.ac.uk

ABSTRACT

PVC foam (Divnycell© H200) was tested under shear loading to mimic the fracture processes which have been observed in mode II delamination growth in carbon fibre reinforced polymer (CFRP) laminates. By varying the cross-section geometry of the foam, different load-displacement behaviours and fracture morphologies were produced. The cross-section geometries considered included variations in the size and shape of longitudinal side grooves in the foam. The influence of pre-cracking was also investigated. Cusp formation was observed to begin with the initiation of a series of inclined cracks distributed along the length of the specimen. Propagation of these cracks resulted in S-shaped ligands and the subsequent deformation of these ligands and coalescence of the cracks resulted in cusp features in the fracture surfaces of the foam. Cusp size was found to be influenced by the height and width of the side grooves and these effects were comparable to those observed in mode II delamination of CFRP due to inter-fibre spacing. The results of this study provide understanding and data which can be used in the development and validation of numerical models of the delamination processes in fibre reinforced laminates. Such models may eventually provide the means for optimisation of the interlaminar fracture toughness of CFRP laminates.

1. INTRODUCTION

As polymer matrix composites have matured as a structural material, the problem of delamination, and how to mitigate for it, has been a recurring theme. Delamination can develop from a number of sources[1] such as manufacturing defects, local stress concentrations and impact damage, and can significantly reduce structural performance[2]. These problems have plagued composite development over the last forty years, hindering the introduction of composites to new applications. Reliable prediction of delamination growth under realistic conditions has proved to be problematic[2-4], leading to the use of large safety factors and a reluctance by designers to utilise composites in primary structural applications. This has resulted in composite structures being perceived as expensive to fabricate and needing frequent inspection and repair incurring significant through-life costs[4].

There has been extensive research on modelling delamination, and the recognised approach is to partition the energy release rate (G) into three modes; opening, shearing and tearing (modes I, II and III respectively)[5,6]. Failure criteria, relating energy release rates in these modes and the associated critical energy release rates (G_C), can then be used to predict whether delamination growth will occur. Although a range of failure criteria have been developed[7-9], most of them are purely empirical with no physical basis. In particular, there is little or no relationship between the fundamental physical mechanisms for delamination growth, and the parameters used in delamination failure criteria. Clearly, if engineers are to have confidence in designing composite structures against delamination, developing criteria with a physical basis is essential. The key to developing physically-based criteria is through fractographic observations[10]; these provide an insight into the dominant failure mechanisms and thus the critical mechanisms can be identified, ranked and appropriately incorporated into a delamination growth criterion.

The focus of the research reported here is to understand the physical processes associated with mode II (shearing) fracture. This is perhaps the most important delamination mode, dominating under conditions such as impact, bending and buckling of laminates. Using a novel macro-scale experimental model, this paper focuses on a key mechanism associated with mode II fracture; cusp formation and deformation[11]. In fact, cusp formation and deformation is thought to be the dominant energy absorbing process during mode II fracture, and is considered to be the principal reason why mode II fracture toughness greatly exceeds mode I fracture toughness in thermosetting CFRPs[12,13]. Investigations by Lee[14] showed that cusp formation is highly influenced by fibre arrangement and resin content. Lee demonstrated that fibre spacing affects the stress concentrations in the neighbouring resin, constraining the region of cusp formation, and that resin plasticity influences the spacing between multiple microcracks, thus dictating the number of cusps able to form through microcrack coalescence.

Microcrack coalescence is not only evident in laminate fracture[14,15] but also in shear-loaded adhesive failure[16]. Theoretically[14-17] multiple microcracks form in resin-rich layers ahead of a crack tip, in a plane normal to the tensile principal stress (i.e. 45˚ to the shear loading direction). As shown in Figure 1, these microcracks tend to form at a spacing (L) apart, due to shear lag effects. These then propagate to form sigmoidal (or S-shaped) ligands which then coalesce across shear bands at either the upper or lower boundary of the resin-rich region. In some instances the microcracks have been observed to have an increased inclination above 45˚, thought to be a result of cusp rotation due to shear loading before the final coalescence of the microcracks[15]. In other cases the inclination is much shallower, the reasons for which are currently unclear[16].

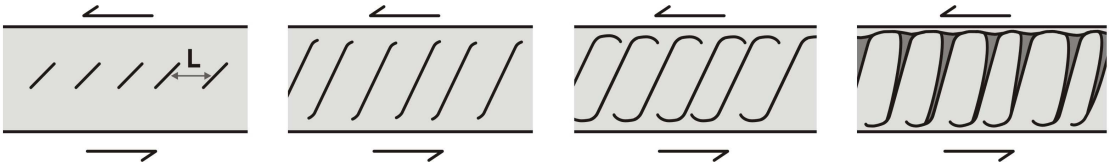


Figure 1: left-right (a) microcracks form at spacing L apart (b) microcracks propagate towards the interface to form S-ligands (c) S-ligands coalesce through shear bands in the top and bottom of the material and finally (d) Coalesced ligands form cusps that rotate as shear continues.

Due to the microscopic scale of cusps, it is very difficult to study the initiation and propagation processes in-situ. However, it has been observed that PVC foam material tested under shear loading produces similar fracture morphology to that generated in mode II loaded CFRP laminates[18], but at a much larger scale, as shown in Figure 2.



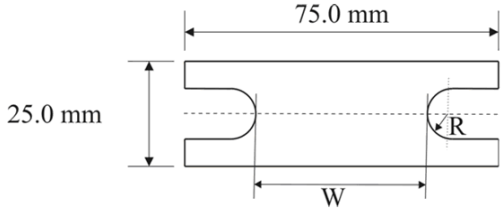
Figure 2: Cusp features on the fracture surfaces of (a) a benchmark PVC specimen (cusp 20mm) and (b) an epoxy based CFRP laminate (cusp 5μm)[11].

For this reason, shear testing of PVC foam was chosen as a means to characterise and understand the cusp formation processes, and to provide an insight into the parameters which control their morphology. Measurement of the load-displacement behaviour of the material during cusp formation will provide experimental data for validation of

numerical micromechanical models of mode II fracture. Such models would then provide a physical basis for developing predictive models of mode II interlaminar toughness of CFRPs.

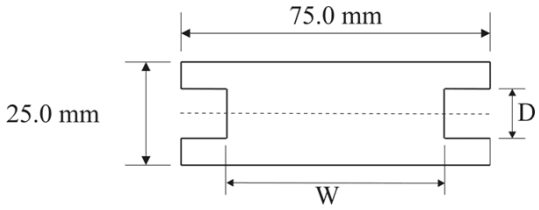
2. EXPERIMENTAL PROCEDURE

Divinycell© H-grade PVC foam, H200, was tested in shear using the ASTM standard test method C-273[19]. This material had an average density of 200kg/m^3 and shear modulus of 85MPa[20]. The benchmark specimen for this study (Figure 3) had a cross-sectional profile radius of curvature (R) 6mm, width (W) 41mm and length 300mm. This configuration was identical to that of the specimens that had been observed to produce cusp-like features on their fracture surfaces following shear loading[18]. Five, nominally identical, benchmark specimens were tested.



Specimen Name	R (mm)	W (mm)
Benchmark	6.0	41.0
Curve-5	2.5	41.0
Curve-15	7.5	41.0
Width-31	6.0	31.0
Width-51	6.0	51.0

Figure 3: Cross-section of the curved-profile specimen and tabulated dimensions corresponding to the curvature (R) and width (W).



Specimen Name	D (mm)	W (mm)
Square	12.0	41.0
Flat	-	75.0

Figure 4: Cross-section of the square-profile specimen and tabulated dimensions corresponding to the depth (D) and width (W).

To develop an understanding of the effects of profile dimensions on the frequency, morphology and size of the cusp features on the PVC foam fracture surface, three specimens of each of the four additional configurations shown in Figure 3 were tested. It was anticipated that the curvature (R) and width (W) would possibly mimic the influence of fibre radius and the inter-fibre spacing respectively, in CFRPs. The effect of profile shape on the cusp morphology was further investigated by testing specimens of both flat and square-profile, as illustrated in Figure 4. The influence of pre-cracking on the failure mechanisms was also investigated using specimens of the benchmark configuration.

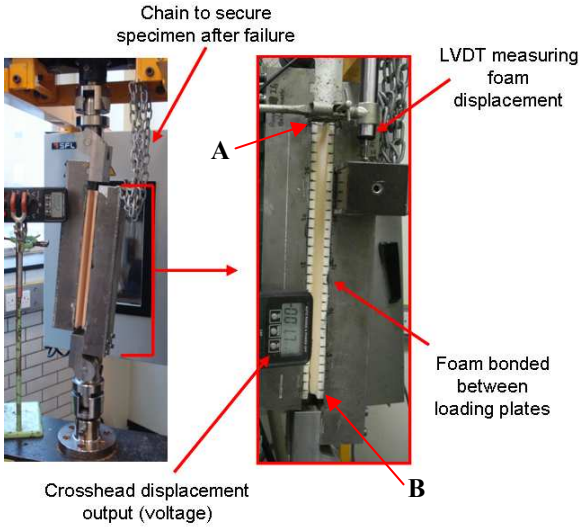


Figure 5: Benchmark specimen and test fixture in the loading frame.

Each specimen was bonded between two milled steel loading plates using Araldite 420 cured at room temperature for at least 24 hours. The loading plates and fixtures used were manufactured according to the ASTM C-273 Standard[19]. All the tests were carried out at room temperature under displacement control, at a crosshead displacement rate of 3mm/min using a 100kN Instron loading frame. This rate ensured that failure occurred between three to six minutes after the start of the test. During testing a linear variable displacement transducer (LVDT) was used to measure the specimen deflection, by measuring the difference in displacement of the loading plates according to the test standard[19], and thus the load-displacement response of each specimen was characterised (Figure 5). Two video cameras were used to simultaneously capture the fracture process on both sides of the specimens. The images from the cameras were correlated directly with the load-displacement response from each test.

3. EXPERIMENTAL RESULTS

The results of these experiments are summarised in this section. Firstly, a detailed analysis of the typical failure processes and fracture morphologies in the benchmark is described in Section 3.1. This is followed by a description of the influence of pre-cracking, profile shape, curvature and width, on these processes and morphologies, in Sections 3.2 to 3.5 respectively. A summary of the results are presented in Figure 6 and Figure 7.

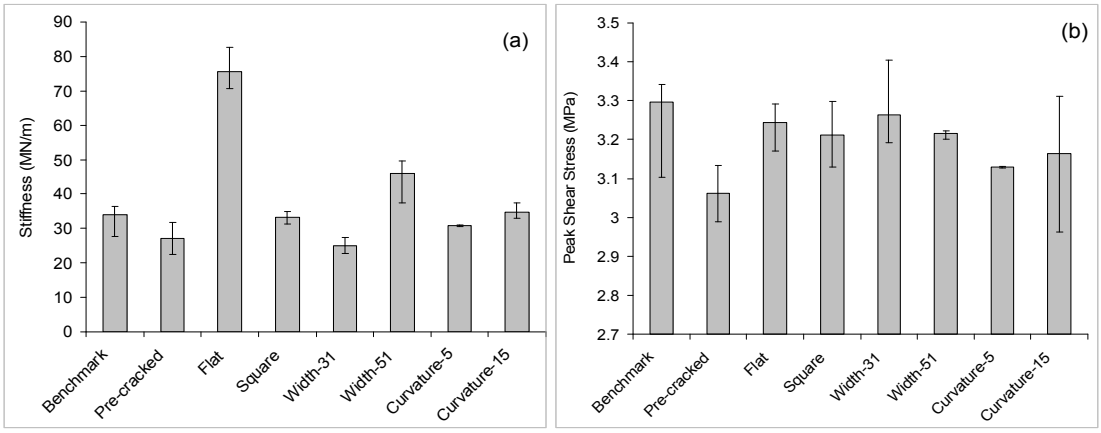


Figure 6: Bar graphs representing average data for each specimen configuration for (a) initial stiffness (MN/m) and (b) peak shear stress along the mid-plane (MPa). (Error bars showing maximum and minimum value.)

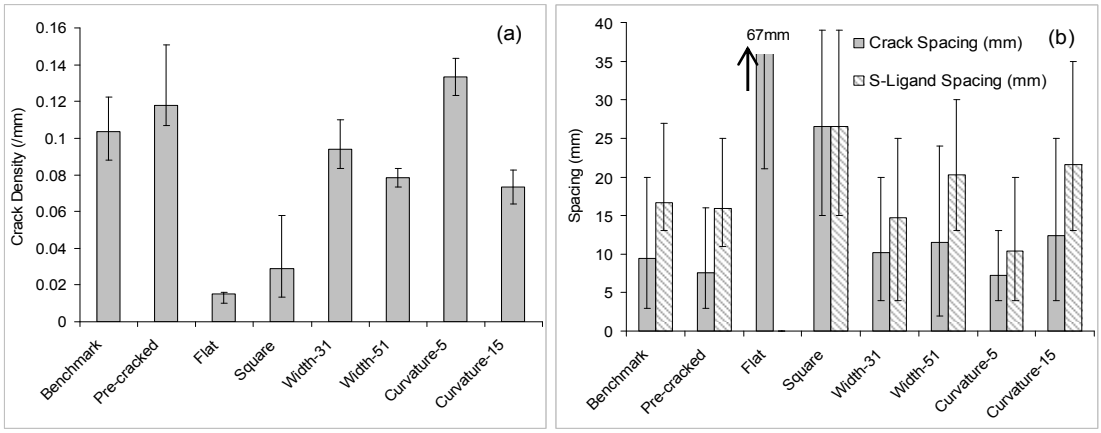


Figure 7: Bar graphs representing average data for each specimen configuration for (a) crack density (/mm) and (b) the spacing between cracks and S-ligands (mm). (Error bars showing maximum and minimum value.)

3.1 Benchmark Configuration

The results of the benchmark tests are presented in Figure 6 and Figure 7, and the typical load-displacement response for the benchmark configuration is represented in Figure 8, which also depicts the points of crack initiation and saturation.

Initially the load-displacement slope (Figure 8) is essentially constant with an average stiffness of 34.1MN/m (Figure 6a). At approximately 35kN an onset of non-linearity was observed in the load-displacement response leading to a significant drop in stiffness, to an average value of 1.2MN/m. This was thought to arise from a combination of material plasticity and some peeling of the foam from the loading plates at either end of the specimen. This issue is discussed in more detail later. The load-displacement response continued to increase linearly until the first cracks initiated at an average applied displacement of 0.6mm (range 0.3-1.0mm) less than that at the maximum load, labelled as the point of *crack initiation* on Figure 8. These cracks initiated on the specimen faces along the mid-plane and were approximately parallel. It was not possible to discern the exact angle of crack initiation, with respect to the load plates, but as the cracks propagated is was possible to measure inclinations that laid between 40˚ and 60˚.

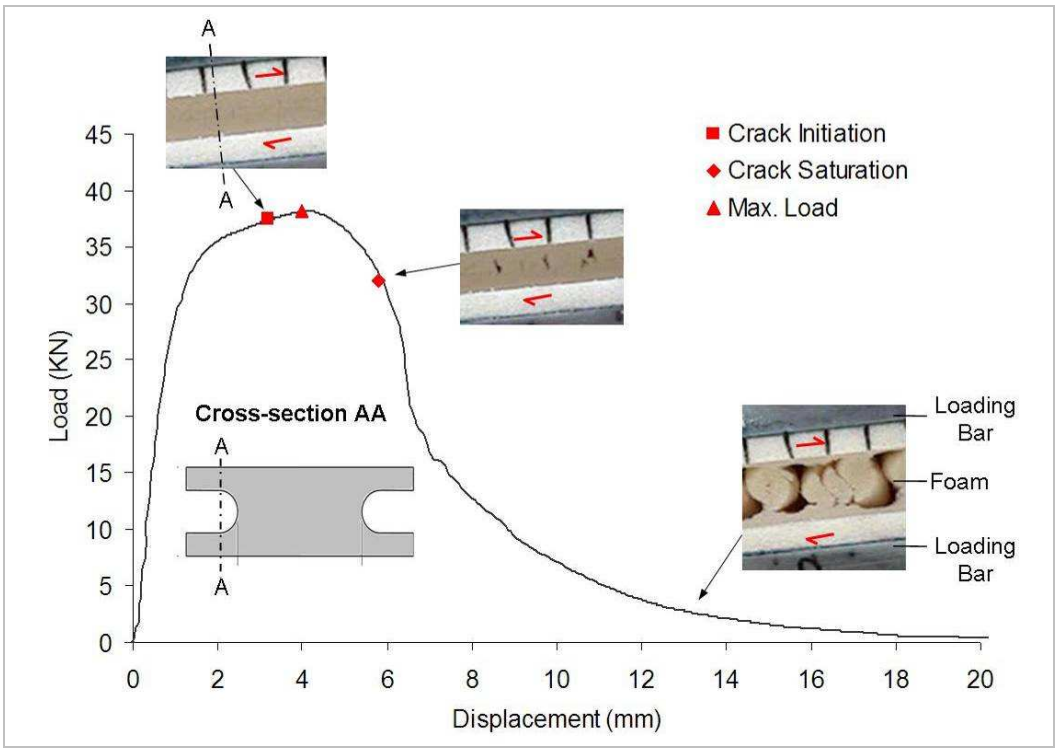


Figure 8: Fracture morphologies depicted on a typical load-displacement plot for a benchmark specimen; 10mm increments are marked on the images.

After *crack initiation* the number of cracks increased up to a point of *crack saturation* on the load-displacement response, at an average applied displacement of 1.25mm (range 0.6-2.0mm) after the maximum load (Figure 8). Shortly after *crack saturation* an inflection was observed in the load-displacement response. Some cracks continued to propagate towards the interface between the foam and the loading plates whilst others closed or coalesced to form “crows-feet”, as discussed later. As the crack faces opened up, S-shaped ligands developed that bridged the specimen thickness and consequently, at displacements in excess of 12mm, cusps were formed via the rotation and detachment of the S-ligands. During the formation of the cusps the load continued to decay.

During the fracture process it was noticed that the spacing of the initiating cracks was not uniform along the specimen length and that some cracks developed into S-ligands before crack saturation occurred. After testing, examination of the fracture surfaces in more detail revealed that the crack density averaged 0.104cracks/mm, with an average crack spacing of 9mm although this varied from 3mm to 20mm (Figure 7b). It was also noted that not all of the cracks led to the formation of S-ligands. Typically, there was an average of fifteen S-ligands per specimen with an average spacing of 17mm (Figure 7b). The cracks that did not form S-ligands tended to form "crows-feet"[10], that initiate from multiple microcracks at the edge of the cusp that merge together, as visible in Figure 9b.

It was observed that peeling of the foam from the loading plates occurred at both ends of the specimens, prior to crack initiation. This peeling occurred along the loading plate/foam interfaces labelled A and B in Figure 5. Peeling was heard to initiate at approximately the same time as the onset of non-linearity in the load-displacement response (Figure 8), but was not visually observed until after this time. The peeling at each end of the foam extended no more than 25mm along the specimen/loading plate interface and coalesced with the cracks that formed at each end of the specimen length between *crack initiation* and *crack saturation*. Investigations into the peeling using finite element analysis found that only a small reduction in the stiffness was due to this effect; a 25mm peeled length, at each end of the specimen, resulted in a 0.6% reduction in the stiffness. Therefore, the observed fall from 34.1MN/m to 1.2MN/m implied that plasticity of the foam dominated the load-displacement response following the onset of non-linearity.

Post-test observations (Figure 9) revealed the cracks had extended straight across the width of the specimen having propagated in from the edges via S-ligands. Cracks that did not form S-ligands joined together to produce "crows-feet"[10], at the specimen faces as labelled in Figure 9. Most of the foam fracture surface remained attached to the uppermost loading plate, with an imprint similar to "scallops"[10], visible on the lower loading plate, where the material forming the cusps had been removed. The cusp, "crows-feet" and "scallop" features observed on the benchmark configuration were all similar to those observed in mode II interlaminar failure of CFRP (Figure 2).

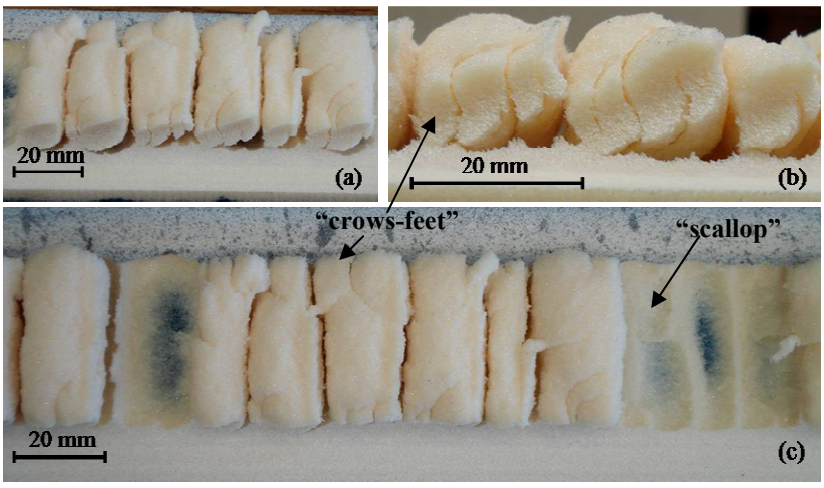


Figure 9: Fracture surface of a typical benchmark specimen from (a) aspect view (b) side view and (c) plan view.

3.2 Influence of pre-cracking on the fracture processes

Three benchmark specimens were pre-cracked at the mid-plane at one end to mimic the conditions in CFRP mode II fracture toughness coupons and to determine whether the crack spacing would be influenced by proximity to the crack tip. A pre-crack length of 70mm was cut in the foam using a razor blade. The pre-cracked specimens fractured in a similar manner to the benchmark specimens through the formation and

coalescence of S-ligands to form cusps. The initial stiffness of the load-displacement response was smaller for the pre-cracked configuration (Figure 6a and Figure 10) and the load at onset of non-linearity in the response was approximately 25% lower for the pre-cracked specimen, which was consistent with the 23% reduction in the mid-plane area of the specimen. The difference in peak shear stress from the benchmark was negligible. Crack initiation and crack saturation were observed to occur closer to the maximum load than for the benchmark specimens.

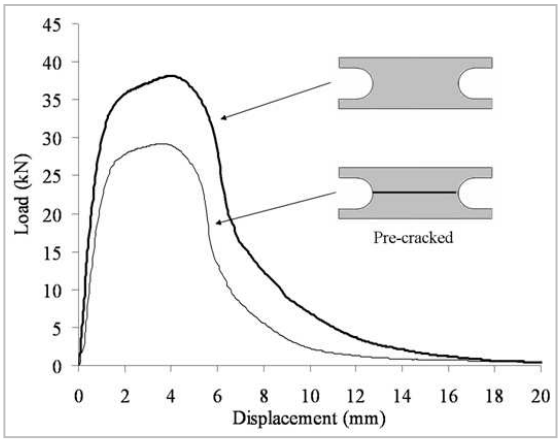


Figure 10: Typical load-displacement response representing the effects of pre-cracking (benchmark specimen in bold).

The introduction of the pre-crack produced a slight increase in the average crack density and thus a decrease in the average spacing between S-ligands from 17mm, in the benchmark, to 15mm, in pre-cracked specimens (Figure 7) but in view of the scatter this is not thought to be significant. Further investigation revealed that introduction of the pre-crack slightly improved the uniformity of the crack spacing in the region closer to the crack tip. As the distance from the crack tip increased along the specimen length, crack spacing became more varied. The crack spacing in the benchmark specimen was non-uniform along the entire specimen length. However the scatter made it impossible to draw clear conclusions regarding the influence of a pre-crack on crack initiation in PVC foam.

3.3 Influence of profile-shape on the fracture process

The effect of profile shape was considered by comparing both flat and square-profile configurations (Figure 4) against the benchmark specimen. Figure 6a and Figure 11 demonstrate that both the benchmark and square-profile specimens had similar initial stiffness, whereas the flat specimen showed a 122% increase in the initial stiffness by comparison. The initial stiffness of the flat specimen is higher than the benchmark and square configurations because of the flexibility that is introduced by the side grooving. Following the onset of non-linearity in the load-displacement response, each configuration developed a second linear phase with much reduced stiffness, with the flat specimen exhibiting the highest stiffness (Figure 11). For the flat and square profile specimens, the load-displacement response after the peak load differed from that of the benchmark specimens (Figure 11). In the benchmark specimens the load/ displacement slope gradually became more negative as the applied displacement increased, becoming steepest around the point of crack saturation and then the slope became gradually less steep as the load reduced to zero. However in the flat and square specimens the load-displacement fell off rapidly after the maximum load,

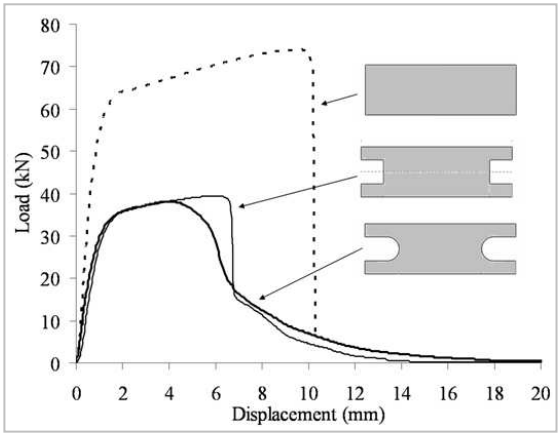


Figure 11: Typical load-displacement response representing the effects of profile shape (benchmark specimen in bold).

leading to catastrophic failure in the flat specimens. In the square specimens this instability in the load-displacement response was arrested as it crossed the benchmark response, and then approximately followed the benchmark response. The peak average shear stress, developed at the specimen mid-plane, was not found to vary significantly with profile shape (Figure 6b). Finally, in the flat and square profile configurations, crack initiation occurred after peak load (unlike in the benchmark case), and, given the instability in crack growth observed in these specimens, this may have significantly influenced the crack density; the benchmark averaged 0.104cracks/mm, flat profile 0.015cracks/mm and square profile 0.029cracks/mm (Figure 7a).

As shown in Figure 12 the change in profile shape had a considerable influence on the fracture morphologies. For the flat profile specimens (Figure 12c and 12d), cracks were observed to extend across the entire thickness with crack initiation occurring just after the maximum load. These cracks ranged from a spacing of 18mm to 90mm, did not form S-ligands, and consequently did not form cusps. The unstable nature of the crack propagation in flat-profile specimens resulted in fairly straight cracks for which the angle, relative to the fixed loading plate, was readily measured to be 61°. In the square-profile specimens (Figures 12e and 12f) crack initiation occurred just after the peak load. These cracks were S-shaped with an average spacing of 27mm, but did not coalesce to form cusps similar to the benchmark (Figure 7b). They also propagated in an unstable manner across the thickness of the side-grooved part of the specimen at an angle of approximately 64° to the fixed loading plate.

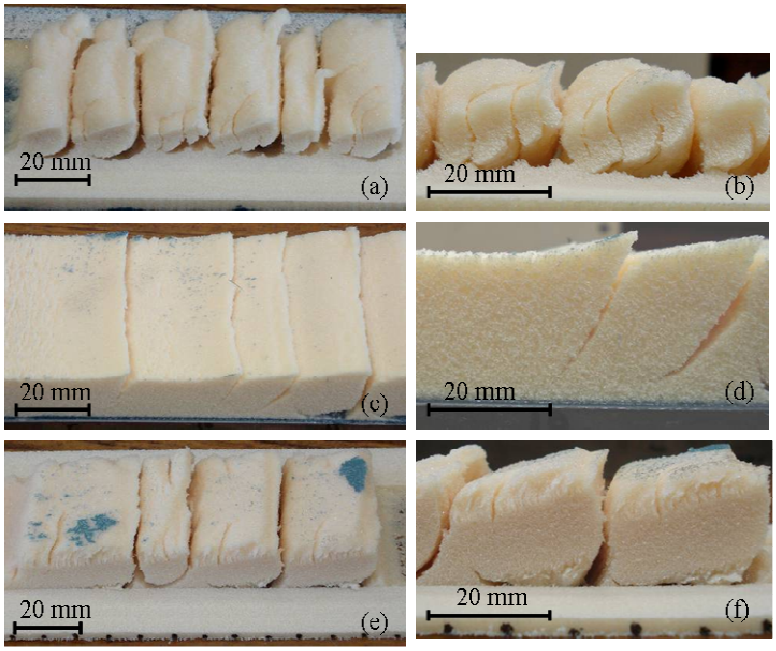


Figure 12: Aspect (left) and side views (right) of the fracture surfaces of (a,b) benchmark, (c,d) flat and (e,f) square profile configurations.

After complete failure of the specimen, small tuft-like features, 2 to 4mm in width, were observed at the crests of the cusps in the upper half of the specimen thickness. These cracks were not visible during testing and did not propagate across the thickness of the specimen side-groove, implying that they had formed along the right angled corner of the 'square' side groove. Similar to the benchmark specimens, the cracks initiated on the specimen faces and propagated inwards.

3.4 Influence of curvature on the fracture process

The effect of profile radius of curvature (R) was considered by comparing the benchmarks (R=6mm) to the curvature-5 (R=2.5mm) and curvature-15 (R=7.5mm) configurations as depicted in Figure 3. The typical load-displacement responses for each configuration (Figure 13) were similar with a slight, but not significant, increase in the initial stiffness as the R dimension decreased (Figure 6a). As with the previous

configurations, the peak average shear stress at the mid-plane did not seem to vary significantly with R (Figure 6b). Crack initiation occurred 0.8mm prior to the peak load in the curvature-15 specimens compared to an average of 0.6mm for the benchmark and curvature-5 specimens, whilst crack saturation occurred 1.0mm after the peak load in the curvature-5 specimens and 0.8mm after in the curvature-15 specimens compared to an average of 1.25mm in the benchmark specimens.

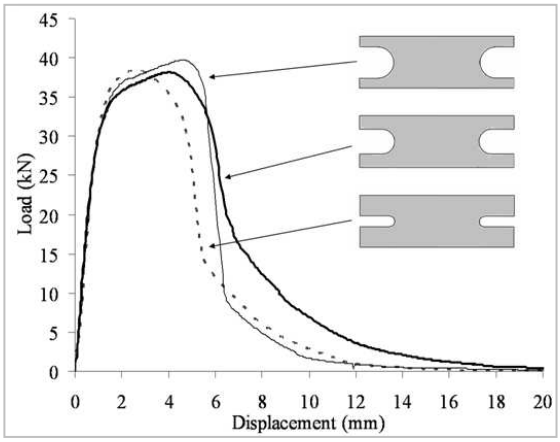


Figure 13: Typical load-displacement response representing the effects of curvature, R (benchmark specimen in bold).

The fracture of each configuration occurred in a manner similar to the benchmark specimens via the initiation and coalescence of S-ligands. Figure 14 demonstrates that both the cusp depth (size along the specimen length), and height (size in the direction of the specimen thickness) increased with profile radius of curvature (R). This was consistent with a decrease in the crack density from 0.133cracks/mm to 0.073cracks/mm, and an increase in the S-ligand average spacing from 10mm to 22mm, for curvature-5 and curvature-15 (Figure 7). It was also observed that the number of crows-feet on the specimen edges decreased as the radius of curvature (R) increased (Figure 14); i.e. the cusps become more block like.

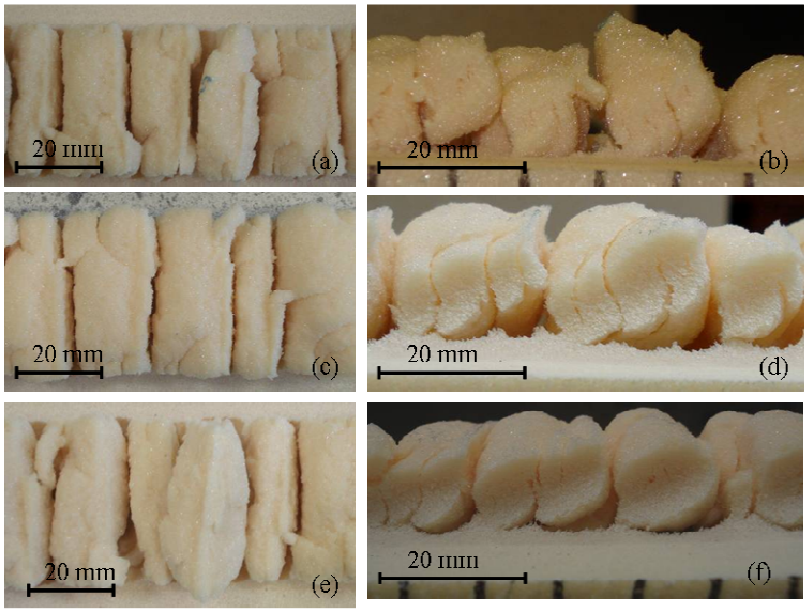


Figure 14: Fracture surface from plan view (left) and side view (right) of (a-b) curvature-5, (c-d) benchmark and (e-f) curvature-15 configurations.

3.5 Influence of width on the fracture process

The effect of the foam width (W) was considered by comparing benchmark specimens (W=41mm) with two configurations; width-31 (W=31mm) and width-51 (W=51mm) as depicted in Figure 2. As can be seen in (Figure 6a), the initial stiffnesses increased proportionally with the width (W), and each configuration (Figure 15) exhibited a similar response after the onset of non-linearity. The peak average shear stress at the mid-plane did not seem to vary significantly with W (Figure 6b). Crack initiation occurred at an average of 0.3mm and 1.0mm before the maximum load, and crack saturation occurred at an average of 0.8mm and 0.6mm after the maximum load for width-31 and width-51 specimens, respectively. These can be compared to the average benchmark specimen data with crack initiation at 0.6mm before and crack

saturation at 1.25mm after, the maximum load. However, as the width increased, the later stages of fracture tended towards those of the flat profile specimen, with a rapid load drop following crack saturation.

Analysis of the fracture surfaces (Figure 16) indicated that cusp depth increased as the width (W) increased but the cusp height remained constant. This was consistent with an increase in S-ligand spacing from 15mm (width-31), 17mm (benchmark) to 20mm (width-51) specimens (Figure 7b). However a discrepancy in the trend of the number of cracks forming along the fracture surfaces was observed, where an increase in the width did not correlate to a decrease in the number of cracks formed (Figure 7a). It was also observed that the number of crows-feet on the specimen edges decreased as the width increased.

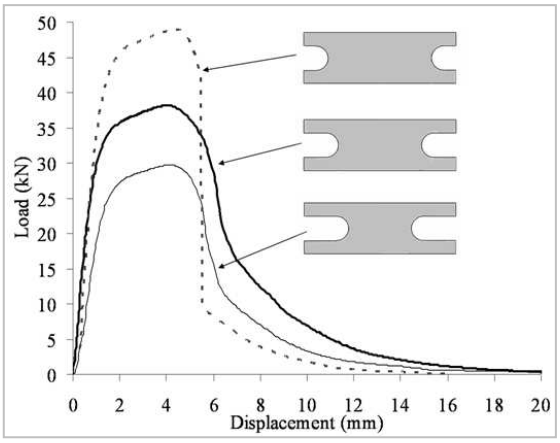


Figure 15: Typical load-displacement response representing the effects of width, W (benchmark specimen in bold).

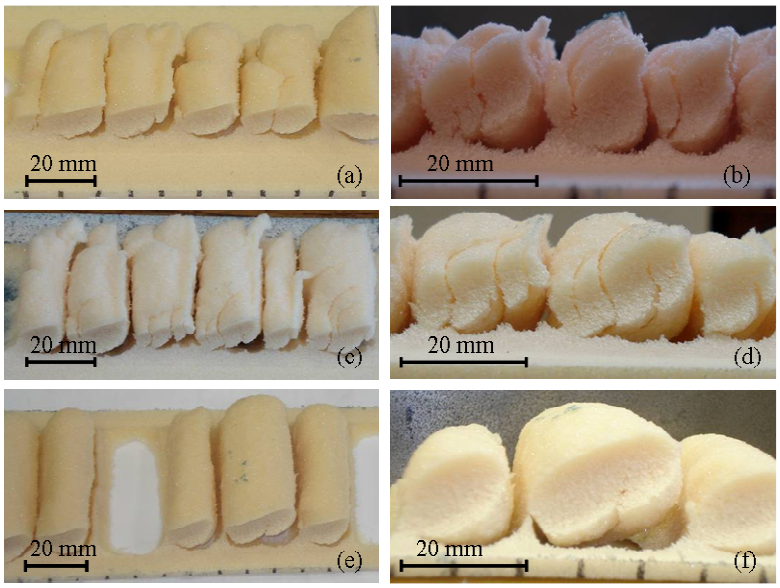


Figure 16: Fracture surface from aspect view (left) and side view (right) of (a-b) width-31, (c-d) benchmark and (e-f) width-51 configurations.

4. DISCUSSION

4.1 General comments on the testing

The damage processes were recorded simultaneously on both specimen faces, and correlated with the load-displacement response, and it was found that in most tests the development of the cracking was the same on both faces. One difficulty which was encountered was associated with peeling of the foam from the loading plates early in the test. The exact load at which peeling initiated could not be visually discerned, but it appeared to coincide with the onset of non-linearity in the load-displacement response. However, this peeling did not extend for more than 25mm and did not appear to significantly influence the specimen compliance.

4.2 Load-displacement response

Results for each specimen configuration indicated that pre-cracking, profile shape and width had the most influence on the load-displacement response, with curvature having slight influence by comparison. The peak average shear stress at the mid-plane was not significantly influenced by the parameter variations studied here, suggesting that the initiation of failure of the foam was in-sensitive to the stress concentrations associated with the profile. Most of the configurations produced similar load-

displacement response as the benchmark, in that no sudden drops were observed in the responses indicating stable damage developments in the specimens. An exception to this was observed in the flat, square and width-51 configurations that showed varying amounts of instability after the maximum load was reached. All the specimens that exhibited an inflection after the point of *crack saturation*, in the load-displacement response, also developed cusps.

4.3 Cusp formation

Results showed that cusp formation occurred in all curved and square profile configurations, but not in the flat profile configuration; i.e. the stress concentration associated with the recess in the profile was required for cusp development. It was also noted that cusps in the curved profile specimens (namely benchmark, curvature and width) all developed from the specimen mid-plane. However, in the square profile specimens, the cusps developed at the 90˚ corner at the upper edge of the 'square' side groove. These cracks initiated at the site of highest stress on the specimen faces, and propagated inwards towards the mid-width.

In all the curved-profile specimens it was evident that a number of randomly spaced cracks initiated along the specimen length, grew into S-shaped ligands and eventually coalesced to form cusps. Whilst these fracture processes generally supported the mechanisms depicted in Figure 1, it was apparent that the crack spacing was far from regular[17]. Furthermore, the introduction of a pre-crack only had a limited influence on the uniformity of the crack spacing and the peak average shear stress, implying that the foam was fairly notch insensitive. This could mean that local variations in the foam properties, induced during manufacture of the material or the specimens, accounted for the large variations in crack spacing.

It was also observed that cracks formed in an unstable manner in the flat and square-profile configurations across the thickness with average inclinations of 61º and 64° respectively, relative to the loading plates. In the benchmark, curvature and width specimens it was not possible to identify the initial inclination of the cracks, but in the region between *crack initiation and crack saturation* the inclinations of the cracks were observed to be between 40˚ and 60˚. The cracks observed in the flat and square specimen both contradict the hypothesis that shear cracks and form normal to the direction of tensile principal stress (i.e. at 45˚ to the shear load direction)[14-17]. However other researchers have observed cusp inclinations both greater than and less than the expected 45°. In particular Hibbs, *et al*[15] observes cusp angles greater than 45° and proposes that these arise due to a rotation in the cusps before microcrack coalescence occurs. In contrast, Leffler[16] observed the presence of ligaments with an angle less than 45˚ when testing thin adhesive layers, and commented that deformation of the adhesive layer was via mixed mode I/II despite being loaded under pure shear. Leffler[16] suggests that the peel deformation contributing to this mixed mode I/II was induced by the adherends moving apart to accommodate the formation of cracks in the adhesive. A similar opening movement was witnessed between the steel loading plates during this study, in all but the flat and square profile specimens, which suggests that a mode I component may be involved in the cusp formation processes. The extent to which this movement influences the energy needed for cusp formation requires further investigation.

It was apparent that the cusp depth was influenced by both the radius of curvature (R) and width (W). As both of these parameters were increased, the cusp depth also increased, consistent with an increase in the S-ligand spacing and decrease in the

crack density. In particular, comparisons between the curved profiles revealed that *crack initiation* and *saturation*, with respect to the maximum load, were mainly influenced by width (W) whilst S-ligand spacing and number of cracks was mainly influenced by curvature (R).

4.4 Implications of present results for delamination in fibre reinforced composites

As discussed in Section 1, the objective of this research was to develop an insight into the key mechanisms (cusps) which contribute to mode II and mixed-mode toughness of continuous fibre composites. To this end, the morphologies produced in this study exhibited strikingly similar features to those observed in polymer composites. In particular, the shape of the cusps, and fractographic features such as "crows-feet" and "scallops" were observed[10]. Furthermore, the prevalence of these features was dependent upon the specimen profile, suggesting these results could provide a route to characterising the mechanisms associated with cusp formation. In the experiments reported here only specimens with a curved profile generated cusps comparable to those in CFRP laminates (Figure 2), which suggests that the curvature of the fibres plays an important role in the cusp formation process. It also suggests that the profile radius of curvature (R) may be used to represent the fibre diameter in CFRPs and the profile width (W), the inter-fibre spacing.

Research by Lee[14,17] indicated that cusps form in regions of high stress concentration between fibres, in an "effective resin layer" as depicted between the dotted region in Figure 17. According to Lee, cusp spacing is proportional to the inter-fibre spacing, such that smaller fibre spacing results in thinner "effective resin layers", and hence produces smaller cusps. The present research on foam fracture supports this suggestion since the cusp depth and S-ligand spacing were observed to decrease with width (inter-fibre spacing) of the specimens. The same influence of inter-fibre spacing was noted by Davies, *et al* [21] where an increase in the inter-fibre spacing, due to a reduction in fibre volume fraction, allowed the development of plastic deformation and matrix micro-cracking. This produced larger cusps and an increase in mode II fracture toughness. Similarly work by Russell[6] indicated that an increase in inter-fibre distance caused an increase in cusp size, which in turn contributed to an increase in the spacing between cracks.

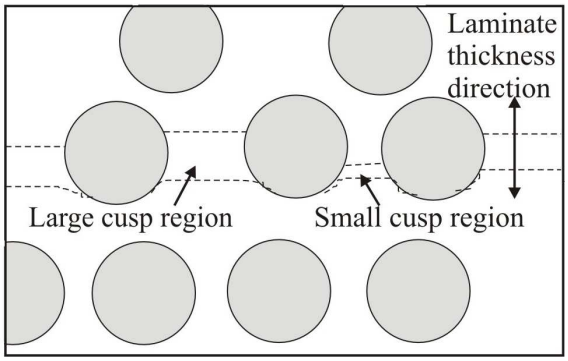


Figure 17: Cross-section showing the crack path and regions of cusp formation between fibres, under mode II fracture[1]

5. CONCLUSIONS

PVC foam (Divnycell© H200) was tested under shear loading using the ASTM Standard C-273[19] to mimic the fracture processes which have been observed in mode II delamination growth in CFRP laminates. By varying the profile geometry of the foam, different load-displacement behaviours and fracture morphologies of the foam were produced. The effects of pre-cracking, profile shape, curvature and width on the behaviour, failure mechanisms and fracture morphology of the foam were investigated. The influence of these parameters was compared to a benchmark configuration and the following conclusions were drawn from these studies.

1. Cusp development comparable to that in CFRPs was observed in curved-profile configurations only, suggesting that the curvature of fibres plays an important role in cusp formation. In this study cusps formed via the propagation and coalescence of sigmoidal (or S-shaped) ligands that initiated as a series of parallel cracks along the specimen length.
2. The experimental studies successfully characterized the load-displacement behaviour during shear cusp initiation, extension and deformation in the foam, and the influence of geometric parameters on this behaviour was determined.
3. The average peak shear stress at the mid-plane of the specimen profile was not strongly influenced by the parameters studied here.
4. Fractographic features particular to mode II fracture of CFRP, including "crows-feet" and "scallops", were observed. The number of "crows-feet" along the specimen edges decreased as the cusp depth increased.
5. Given the similarities in fracture morphology between CFRP and the curved-profile foam configurations, it is suggested that the profile radius of curvature (R) and width (W) could represent the fibre diameter and inter-fibre spacing in CFRPs, respectively. Increases in both these parameters were observed to influence the cusp size, such that; cusp depth increased with R and W and cusp height increased with R.
6. It is anticipated that the results of this study could be used to validate predictive models of the damage development process during mode II fracture of foam, and thus provide models which could be used to predict the mode II fracture toughness of fibre reinforced polymers

6. FUTURE WORK

The authors will develop the experimental work within this study to investigate cusp formation by including mock 'fibres' within the PVC foam. It is anticipated that the effects of the fibre/matrix interface on cusp formation could thus be investigated. Research by Lee[14] also suggested that plasticity had a considerable effect on the formation and spacing of cracks, and therefore cusp formation in a brittle foam, such as Rohacell© WF110 will also be characterised. In conjunction with the experimental work a numerical model is under development to mimic the experimental observations and ultimately produce a predictive model for mode II delamination in composites.

ACKNOWLEDGEMENTS

The authors would like to acknowledge the support and assistance of Prof. Leif Asp (SICOMP, Sweden), Prof. Janis Varna (Lulea University of Technology, Sweden) and Mr Carl-Johan Lindholm (DIAB, Sweden).

REFERENCES

1- Martin R. Proc of the Inst of Mech Eng. 2000 p. 91-7.
2- Garg A. Delamination – A Damage Mode in Composite Structures. Engineering Fracture Mechanics 1988;29:557-84.
3- Ireman T. Efficient design and certification of advanced composite structures. EDVACOS Final Report. 2001. Report No.: BRPR-CT98-0611 BE97-4359.
4- Heath B. Advanced Structural Efficiency (ADSTREFF) - State of Art Report. 2000. Report No.: BETC-1039.

5- Russell AJ, Street KN. Factors Affecting the Interlaminar Fracture Energy of Graphite/Epoxy Laminates. fourth international conference on Composite Materials; 1982 p. 279-86.
6- Russell AJ. Micromechanisms of Interlaminar Fracture and Fatigue. Polymer Composites 1987;8(5):342-51.
7- Greenhalgh ES. Characterisation of Mixed-mode Delamination Growth in Carbon-Fibre Composites Imperial College London; PhD Thesis,1998.
8- Reeder JR. An Evaluation of Mixed-mode Delamination Failure Criteria. NASA Langley Research Center, Hampton, Virginia 23665; 1992. Report No.: NASA TM 104210.
9- Sela N, Ishai O. Interlaminar Fracture Toughness and Toughening of Laminated. Composite Materials: A Review. Composites 1989;20:423-35.
10- Greenhalgh ES. Chapter 4. Failure Analysis and Fractography of Polymer Composites. Woodhead Publishing Limited; 2008.
11- Grediac M, Dufort L. Experimental Evidence of Parasitic Effects in the Shear Test on Sandwich Beams. Experimental Mechanics 2002;42(2):186-93.
12- Johannesson T, Blikstad M. Fractography and Failure Criteria of the Delamination Process. Delamination and Debonding of Materials; 2006 Jan 12; ASTM STP 876 1985 p. 411-23.
13- O'Brien KT. Composite Interlaminar Shear Fracture Toughness, GIIc: Shear Measurement or Sheer Myth? Composite Materials: Fatigue & Fracture; ASTM STP 1330; 1998 p. 3.
14- Lee SM. Mode II Interlaminar Crack Growth Process in Polymer Matrix Composites. Journal of Reinforced Plastics and Composites 1999;18(13):1254-66.
15- Hibbs MF, Bradley WL. Correlations Between Micromechanical Failure Processes and the Delamination Toughness of Graphite/Epoxy Systems.: ASTM STP 948; 1987 p. 68-97.
16- Leffler K, Alfredsson KS, Stigh U. Shear Behaviour of Adhesive Layers. International Journal of Solids and Structures 2007;44:530-45.
17- Lee SM. Mode II Delamination Failure Mechanisms of Polymer Matrix Composites. Journal of Materials Science 1997;32(5):1287-95.
18- Asp L. SICOMP, Sweden. 2005.
Ref Type: Personal Communication
19- Standard Test Method for Shear Properties of Sandwich Core Materials. Annual Book of ASTM Standards, Vol 15.03; 1994. Report No.: C273-94.
20- Technical Data: Divinycell H. DIAB 2007Available from: URL: http://www.diabgroup.com/americas/u_products/u_prods_2.html
21- Davies P, Casari P, Carlsson LA. Influence of Fibre Volume Fraction on Mode II Interlaminar Fracture Toughness of Glass/epoxy Using the 4ENF Specimen. Composites Science and Technology 2005;65:295-300.